Tangentially active polymers in cylindrical channels

José Martín-Roca[1], Emanuele Locatelli[2], Valentino Bianco[3],
Paolo Malgaretti[4] and Chantal Valeriani[1]

1 Departamento de Estructura de la Materia, Física Termica y Electronica,
Facultad de Ciencias Físicas, Universidad Complutense de Madrid,
28040 Madrid, Spain
2 Department of Physics and Astronomy, University of Padova, Via Marzolo 8,
I-35131 Padova, Italy and INFN, Sezione di Padova,
Via Marzolo 8, I-35131 Padova, Italy
3 Faculty of Chemistry, Chemical Physics Department, Complutense University of Madrid,
Plaza de las Ciencias, Ciudad Universitaria, Madrid 28040, Spain
4 Helmholtz Institut Erlangen-Nürnberg for Renewable Energy (IEK-11),
Forschungszentrum Jülich, Cauer Str. 1, 91058, Erlangen, Germany

Abstract

We present an analytical and computational study characterizing the structural and dynamical properties of an active filament confined in cylindrical channels. We first outline the effects of the interplay between confinement and polar self-propulsion on the conformation of the chains. We observe that the scaling of the polymer size in the channel, quantified by the end-to-end distance, shows different anomalous behaviours under different confinement and activity conditions. In particular, we report scaling exponents that are markedly different from their passive counterparts. Interestingly, we show that the universal relation, describing the ratio between the end-to-end distance of passive polymer chains in cylindrical channels and in bulk is broken by activity. Finally, we show that the long-time diffusion coefficient under confinement can be rationalised by an analytical model, that takes into account the presence of the channel and the elongated nature of the polymer.

Contents

1 Introduction

Active systems are characterized by the presence of mechanism that breaks equilibrium at the microscopic scale, generating directed (self-propelled) motion [1]. As a consequence, they display dynamical and collective properties that are vastly different from those displayed by their passive counterparts [2]. Of particular interest, for biological as well as for synthetic systems, is the behaviour of active matter in complex or confined environments [3]. For example, since the seminal work of Rotschild [4] we know that sperm cells accumulates at boundaries, a behavior that is common to bacteria [5, 6] and algae [7]. Such behavior has also been reported for theoretical models that capture the far-field velocity profile of microswimmers under confinement [8, 9], and for both theoretical and experimental results dealing with phoretic colloids [10]. Recently, the characterization of active filaments has become a cutting edge research in active matter [11], for two main reasons. Firstly, systems composed by active polymer-like units are ubiquitous in Nature at different lenght scales, from the sub-cellular level [12–15], to bacteria or other micro-organisms [16–19] all the way to worms and other multi-cellular organisms [20–25]. Secondly, thanks to technological progress, the synthesis of artificial active chains [26–29] and soft robots [30, 31] is now possible. Such synthetic analogues have various possible applications [32, 33].

From the modeling perspective, active polymers are macromolecules composed by out-of-equilibrium beads, whose activity can arise from a temperature mismatch [34–36] or from a self-propulsion force, completely random [37] or oriented along the polymer backbone [38–47]. We focus on the latter case, sometimes also referred to as polar active polymers, as they are believed to mimic the action of molecular motors [48]. Despite the growing interest in the field, few works have investigated the properties of active filaments under confinement. Notably, the effects of spherical confinement have been considered for different models [13,49–52]: spherical confinement is indeed relevant for biophysical systems such as chromatin. Further, the dynamics in complex confinement, such as porous media, has received some attention [53–57]. Other settings, such as translocation [58], slab [59] or cylindrical confinement [60–62] have been rather overlooked. This is surprising, given that understanding the effects of cylindrical and slab confinement has paved the way for understanding more complex scenarios, for passive polymers and active matter alike [3, 63–65].

In this paper we investigate the conformation and dynamics of tangentially active polymers under cylindrical confinement (as shown in Fig. 1). We will show that, as compared to their passive counterparts, the configurational properties of polar active polymers display a rich scenario, that stems from the interplay between confinement and activity. Importantly, these polymers do not follow the same universal curve, reported in the passive case [66]. This suggests that the blob picture, that holds for polymers in equilibrium, is no longer valid and, similarly to Ref. [60], the polymer self-similarity is broken at some non-trivial length scale. We also show that, at variance with active colloids, confinement does not always lead to accumu-
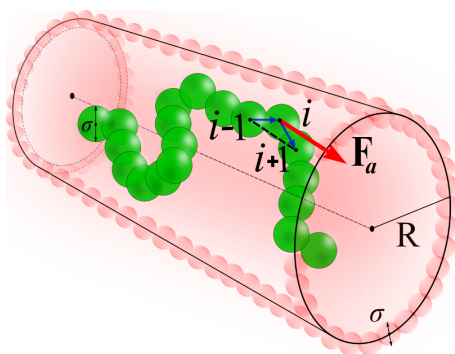
Figure 1: Schematic sketch of the active polymer in a cylindrical channel. Polymer is constructed as beads connected by linear springs. For each bead i the active force is applied in the direction of the vector $(\mathbf{r}_{i+i} - \mathbf{r}_{i-i})/|\mathbf{r}_{i+i} - \mathbf{r}_{i-i}|$. Note that the channel confinement is implemented as a collection of beads. As such, the channel is rough and not perfectly smooth. For visualize propose in the figure the beads of the polymer are bigger than the particles forming the channel.

lation to the channel walls. Rather, such accumulation appears only under weak confinement conditions. Finally, we find that the long-time diffusion coefficient along the channel axis is enhanced for long polymers with respect to the bulk value, even in the weak activity limit. By means of an analytical approximation, we show that this enhancement can be rationalized by a "rod-like" effect, that synergizes with the polar self-propulsion force and effectively increases the polymer diffusion.

2 Models and methods

2.1 Numerical model and simulation details

We model active polymer chains in a coarse-grained fashion; a sketch is reported in Fig. 1. We employ the well known bead-spring Kremer-Grest model [67], where each polymer consists of N monomers, that interact with each others via a repulsive WCA potential

$$U^{WCA} = \begin{cases} 4\epsilon\left[(\sigma/r)^{12} - (\sigma/r)^{6} + \frac{1}{4}\right], & r < 2^{1/6}\sigma, \\ 0, & \text{else,} \end{cases} \tag{1}$$

where σ is the monomer diameter and $\epsilon = 10k_B T$, k_B being the Boltzmann factor and T the absolute temperature. Neighbouring monomers along the backbone are held together by a FENE potential

$$U^{FENE} = \begin{cases} -0.5KR_0^2 \ln\left[1 - (r/R_0)^2\right], & r \leq R_0, \\ \infty, & \text{else,} \end{cases} \tag{2}$$

where we set $K = 30\epsilon/\sigma^2 = 300k_B T/\sigma^2$ and $R_0 = 1.5\sigma$. This choice of parameters allows to avoid strand crossings that could be relevant in the measured properties even in the passive case [67]. We introduce the polymer's activity in the form of a tangential self-propulsion force. All monomers, except the first and the last ones, are self-propelled by an active force with constant magnitude F_a: for monomer i, the force $\mathbf{F}_i^a$ reads

$$\mathbf{F}_i^a = F_a \frac{\mathbf{r}_{i+i} - \mathbf{r}_{i-i}}{|\mathbf{r}_{i+i} - \mathbf{r}_{i-i}|}, \tag{3}$$

and it is parallel to the – normalized – backbone tangent [39,41]. Activity is quantified via the adimensional Péclet number, which measures the strength of the self-propulsion in relation to the thermal noise, defined as

$$\text{Pe} = F_a \sigma / k_B T \,. \tag{4}$$

Finally, the active polymers are confined in straight, cylindrical channels. Confinement is provided by as a collection of immobile beads of diameter σ placed around the channel axis at a fixed distance $R + \sigma$ from it; the distance R is, thus, the radius of the channel. The interaction between the beads and the monomers is given by the WCA potential, Eq. (1). Following the same protocol as in [68], the beads are arranged regularly and, at least, they are at contact distance with their nearest neighbours, as to prevent any possible escape of the polymer.

Throughout the work, we consider the monomers as having unitary mass m; we further set σ and the thermal energy $k_B T$ as the units of length and energy, respectively, so that the characteristic simulation time τ is unitary. We perform Langevin Dynamics simulations, in the overdamped regime, disregarding hydrodynamics. We employ the open source package LAMMPS [69], with in-house modifications to implement the tangential activity. We integrate the equations of motion using the Velocity Verlet algorithm and choose time step $\Delta t = 10^{-3} \tau$. In order to ensure the overdamped regime within the range of values of Pe considered, following [42], we set the friction coefficient γ_0 to $\gamma_0 = 1 k_B T \tau / \sigma^2$, if Pe$< 1$ and $\gamma_0 = 10 k_B T \tau / \sigma^2$ if Pe≥ 1.

We simulate polymers consisting of N monomers, with $40 < N < 750$, at different confinement conditions $6 \leq R/\sigma \leq 18$. We further vary the activity between $0.03 \leq$Pe≤ 10 and average over $M = 50 - 100$ independent realisations. The simulation box is orthogonal, with two short sides $L_y = L_z = 2(R + \sigma) + \sigma$ and a long side $L_x = N\sigma$, parallel to the channel axis, chosen to ensure a fully stretched polymer is contained in a single box. The simulation box is periodic along the channel (x) axis.

Initial configurations are prepared from equilibrium simulations in good solvent conditions, performed using the same Kremer-Grest model. When activity is turned on, we first perform simulation runs to reach the steady state, followed by production runs of (on average) $1 \cdot 10^6 \tau$, corresponding to $1 \cdot 10^9$ time steps (snapshots of the systems are taken every $\tau_s = 10^4 \tau$ or 10^7 time steps).

2.2 Structural and dynamical properties

We compute the average square end-to-end distance, defined as the square euclidean distance between the two ends of the polymer chain

$$\langle \mathbf{R_e}^2 \rangle = \langle (\mathbf{r}_N - \mathbf{r}_1)^2 \rangle \,, \tag{5}$$

where the average is performed, in steady state, on time and on different realisations. In the rest of the manuscript we will consider the (average) end-to-end distance $R_e = \sqrt{\langle \mathbf{R_e}^2 \rangle}$.

We will also report the probability of finding the centre of mass of the polymer $\mathbf{r}_{cm} = \frac{1}{N} \sum_{i=1}^{N} \mathbf{r}_i$ inside the channel at a distance r from the centre of the channel, as well as the orientation of the polymer, i.e. computing the angle between the axis of the channel (the x axis in our simulations) and the instantaneous end-to-end vector, which reads

$$\theta = \arccos\left(\frac{\mathbf{R}_e \cdot \mathbf{x}}{|\mathbf{R}_e|} \right) \,. \tag{6}$$

We remark that the probability distribution of the centers of mass is a radial distribution and, as such, we divide the measured probability by the area of the circular corona between r and $r + \Delta r$, Δr being the chosen bin width.

Concerning the dynamics of the chain, we compute the characteristic time scale of the dynamics, τ_e, as the correlation time of the end-to-end vector: we extract τ_e from the end-to-end time autocorrelation function

$$C_{R_e}(t) = \left\langle \frac{\mathbf{R}_e(t_0 + t) \cdot \mathbf{R}_e(t_0)}{|\mathbf{R}_e(t_0)|^2} \right\rangle, \tag{7}$$

by fitting the data at short times with an exponential function $C_{R_e}(t) = \exp(-t/\tau_e)$. The average (in steady state) in Eq. (7) is performed both on the initial time t_0 and on the ensemble of the different realisations. Finally, we compute the mean square displacement (MSD) of the centre of mass along the direction of the channel axis, i.e. along the x axis

$$\langle \Delta x^2(t) \rangle = \left\langle [x_{cm}(t_0 + t) - x_{cm}(t_0)]^2 \right\rangle, \tag{8}$$

where x_{cm} is the position of the centre of mass of the polymer along the channel axis. The average is performed as previously detailed. For times much longer than τ_a, the MSD grows linearly in time. As common in active matter systems, we identify this regime as the long-time active diffusive regime and compute the (long time) active diffusion coefficient D_a as

$$D_a = \lim_{t \to \infty} \frac{\langle \Delta x^2(t) \rangle}{2d\,t}, \tag{9}$$

following the Einstein relation, where $d = 1$ is the effective dimensionality of the system.

2.3 Theoretical modeling

2.3.1 Mapping an active polymer to an active Brownian particle

The mapping between a tangentially-driven active polymer in bulk and an Active Brownian particle (ABP) has been introduced in Refs. [39,42,44]. We extend this mapping to describe the dynamics of an active polymer under confinement. Specifically, we map the dynamics of the centre of mass of the polymer, projected along the axis of the channel, to an ABP in 1D. Briefly, the ABP model is characterised by an active force, $\mathbf{f}_a^{ABP}$, whose magnitude f_a^{ABP} is constant and a self-propulsion direction $\hat{n}$ evolving in time as a stochastic process with a characteristic time, τ_r^{ABP}, usually called reorientational time. In what follows, we will consider an ABP model whose active force evolve by rotational diffusion. In addition, the ABP is subject to thermal noise, with thermal energy $k_B T$ and friction coefficient γ^{ABP}.

In the overdamped limit, the long time diffusion coefficient of an ABP can be expressed as [70]

$$D_a^{ABP} = D^{ABP} + \frac{\tau_r^{ABP} \left(v_a^{ABP}\right)^2}{2d} = D^{ABP} + \frac{\tau_r^{ABP} \left(f_a^{ABP}/\gamma^{ABP}\right)^2}{2d}, \tag{10}$$

where $v_a^{ABP} = f_a^{ABP}/\gamma^{ABP}$ is the self-propulsion velocity and $D^{ABP} = k_B T/\gamma^{ABP}$ the translational diffusion coefficient. Since we consider an ABP in 1D, we set $d = 1$.

In order to map the polymer to an ABP, we have to provide effective values for the friction coefficient, the reorientation time and the active force. For a polymer of length N, the effective friction coefficient on the centre of mass is related to the monomer friction coefficient γ_0, disregarding hydrodynamics, as

$$\gamma_P = N \gamma_0. \tag{11}$$

For the polymer model considered in this study, we approximate the total active force $\mathbf{F}_a = \sum_i \mathbf{F}_i^a$ to be almost parallel to the end-to-end vector of the polymer, $\mathbf{R}_e$

$$\mathbf{F}_a \approx F_a \frac{\mathbf{R}_e}{\sigma}, \tag{12}$$

where σ and F_a are defined in Sec. 2.1. As in Eq. (10), we define the propulsion speed for the effective ABP particle as the ratio between the magnitude of the total active force $\mathbf{F}_a^P$ and the total friction coefficient γ_P

$$v_a = \frac{|\mathbf{F}_a|}{\gamma_P} \approx \frac{F_a}{N\gamma_0}\frac{R_e}{\sigma} = \frac{1}{N\gamma_0}\frac{\mathrm{Pe}\,k_B T}{\sigma}\frac{R_e}{\sigma}\,, \tag{13}$$

where we take $R_e = \sqrt{\langle R_e^2\rangle}$. The thermal contribution to the diffusion coefficient follows from the Rouse model,

$$D_N = \frac{k_B T}{\gamma_P} = \frac{k_B T}{N\gamma_0} = \frac{D_0}{N}\,, \tag{14}$$

$D_0 = k_B T/\gamma_0$ being the diffusion coefficient of single passive monomer. Finally, from Eq. (12) follows that the reorientational time of the active force is equal to the correlation time of the end-to-end vector of the polymer

$$\tau_r = \tau_e\,, \tag{15}$$

where the auto-correlation time of the end-to-end vector τ_e was introduced in Sec. 2.2.

Combining Eqs. (10), (12), (13) and (15), we can write

$$\frac{D_a - D_N}{D_N} = \frac{\tau_r^P D_0}{\sigma^2}\frac{R_e^2}{2N\sigma^2}\mathrm{Pe}^2\,. \tag{16}$$

This expression is equivalent to that reported in Refs. [39,42], but projected in 1D.

2.3.2 Predicting the diffusion coefficient: Bulk estimate and angular correction under confinement

In the bulk, one can take advantage of the scaling relations, reported in Ref. [39]: the end-to-end distance follows

$$R_e^B = \sigma\,\frac{a_{R_e} + h_{R_e}\,\ln\left(\sqrt{\delta_{R_e}^2 + \mathrm{Pe}^2}\right)}{(\mathrm{Pe}+1)^{c_{R_e}}}\,N^{\nu_a^B(\mathrm{Pe})}\,, \tag{17}$$

where a_{R_e}, h_{R_e}, δ_{R_e}, c_{R_e} and $\nu_a^B(\mathrm{Pe})$ are fitting parameters. In the Supplemental Material, we report measurements for R_e^B in the bulk for the model discussed in Sec. 2.1; we verify that the functional form of Eq. (17) remains valid, within the range of parameter considered, with $a_{R_e} = 1.5$, $h_{R_e} = 0.058$, $\delta_{R_e} = 0.0005$, $c_{R_e} = 0.201$ and $\nu_a^B(\mathrm{Pe}) = 0.54\,\mathrm{Pe}^{-0.022}$. Further, an expression for the correlation time of the end-to-end vector is available in the bulk:

$$\frac{\tau_e^B D_0}{\sigma^2} = \tau_0^B\frac{N}{\mathrm{Pe}}\,, \tag{18}$$

with $\tau_0^B = 0.5$. Thus, if we disregard the effect of confinement, we get the following expression:

$$\frac{D_a^B - D_N}{D_N} = \frac{\tau_0^B}{2}\frac{\mathrm{Pe}}{(\mathrm{Pe}+1)^{2c_{R_e}}}\cdot\left(a_{R_e} + h_{R_e}\ln\left(\sqrt{\delta_{R_e}^2 + Pe^2}\right)\right)^2 N^{2\nu_a^B(\mathrm{Pe})}\,. \tag{19}$$

Finally, we include the contribution of confinement by adapting the correction developed in Ref. [71] for rod-shaped particles. We indeed approximate the polymer under confinement as a rod whose main axis is given by the end-to-end vector $\mathbf{R}_e^C$; the maximum angle between $\mathbf{R}_e^C$ and the channel axis indicates the degree of confinement and is used to correct the estimation of the diffusion coefficient. The expression for the diffusion coefficient now reads:

$$\frac{D_a^C - D_N}{D_N} \approx (1 + 2\cos(\theta_{max}))\,\pi\frac{\tau_e^C D_0}{\sigma^2}\frac{\left(R_e^C\right)^2}{3N\sigma^2}\mathrm{Pe}^2\,, \tag{20}$$

where R_e^C is the end-to-end distance under confinement and $\sin(\theta_{max}) = h_0/R_e^C = 2R/R_e^C$. We highlight the addition, with respect to Eq. (16), of a factor 2π to include the contribution caused by the axial symmetry. We remark that R_e^C and τ_e^C are estimated from simulation data (see Sec. 2.2). We report a detailed derivation of Eq. (20) in the Supplementary Material.

3 Results

We first report the scaling properties of the end-to-end vector and discuss a deviation of the numerical results with respect to the passive universal scaling under confinement. We further investigate the position of the polymer inside the channel and its orientation with respect to the channel axis. Then we report on the dynamics of the active filaments, discussing the scaling of the correlation times. Finally, we apply the theoretical mapping, introduced in Sec. 2.3 and compare the predictions against the numerical data. For most observables, we report additional data in the Supplemental Material. In what follows, we will indicate quantities with a superscript C and B for confinement and bulk, respectively; quantities that refer to the passive limit will be also tagged with a p and we will omit the equivalent tag "a" in the active case, for the sake of simplicity.

3.1 Scaling properties of the end-to-end distance

First, we report on the scaling properties of the end-to-end distance R_e^C for active polymers under confinement. R_e^C provides a measure of the polymer extension, taken to be representative of the polymer size under cylindrical confinement. Indeed, passive polymer filaments under uniaxial confinement become more aspherical, as the channel restricts the available space in the plane transverse to its axis. We thus focus on characterising its scaling properties, i.e. how R_e^C grows upon increasing the number of monomers N. For confinement lengths smaller than (or comparable to) the extension of the polymer [65], the scaling of R_e^C for passive, flexible polymers under confinement is characterised by the de Gennes regime. For tangentially active polymers, the scaling in the bulk of R_e^B does not follow the same power-law as in passive systems: a coil-to-globule-like transition appears upon increasing the activity [39, 41, 44, 46]. This implies a decrease of the value of $\nu^B(\text{Pe})$, as compared to the passive value. We should thus expect an interplay between the two opposite trends imposed by activity and confinement. We first discuss, in Fig. 2, the dependence of R_e^C on N for tangentially active linear chains under confinement in two limiting cases of weak (Pe $\ll 1$) and strong (Pe $\gg 1$) activity: specifically, we consider Pe $=0.03$ and Pe $=10$ under strong ($R = 6\sigma$, Fig. 2a) and weak ($R = 18\sigma$, Fig. 2b) confinement conditions. We also report the measured exponents for all the values of R and Pe simulated in the Supplemental Material. We remark that the "strong" or "weak" confinement is not only a feature of the channel, but it is rather given by the ratio between R and the polymer size in the bulk (e.g. R_e^B). We fix R here and vary N, as it is instructive to understand how activity modifies the onset of the strong confinement regime. Further, $R = 6\sigma$ represents a strong confinement for most of the polymer lengths considered in this work, while $R = 18\sigma$ is so only for the largest values of N considered; as such they help focusing on the two different scenarios. Alongside the numerical data, we report the passive end-to-end distance under confinement, $R_e^{C,p}$, computed using the formula reported in [68], as a full line. We further highlight the relevant power law trends in the figure with black dotted lines.

We first discuss the strongest confinement $R = 6\sigma$ (Fig. 2a). For weakly active (Pe $=0.03$) and short chains, R_e^C is not affected by activity and follows $R_e^{C,p}$. Upon increasing N, the two curves display different power law behaviours: $R_e^{C,p} \propto N$, following the De Gennes blob scal-
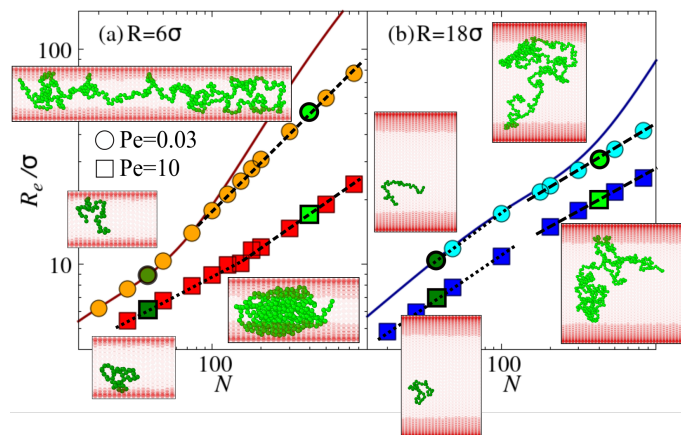
Figure 2: End-to-end distance under confinement R_e^C/σ as a function of N at fixed (a) $R = 6\sigma$, (b) $R = 18\sigma$. In both panels we consider the low activity Pe =0.03 (circles) and high activity Pe = 10 (squares) cases. The full lines is the passive end-to-end distance under confinement $R_e^{C,p}$, computed via the master curve reported in [68]; dashed lines highlight the power law trends in the data.

ing, while R_e^C grows with a smaller exponent, $\nu^C \approx 0.68$; however, notice that ν^C is larger than the exponent for active polymers in the bulk $\nu^B(\text{Pe} = 0.03) \approx 0.56$. We mostly disregard, in this case, the first power law regime due to its limited range; however, notice that R_e^C deviates from its passive counterpart approximately when the strong confinement regime begins ($N \simeq 75$). This is interesting as, for such low values of Pe, tangentially active chains in bulk maintain a coil-like conformation up to $N \sim 150 - 200$ monomers [39], while the confinement considered here affects the conformation already for $N \approx 50$ monomers. This is a first example of the interplay between activity and confinement, that deeply influences both the conformation and the dynamics of the active polymers. At high activity values Pe= 10, we observe that the effect of the activity dominates: R_e^C becomes significantly smaller than $R_e^{C,p}$, even for short chains. Upon closer inspection, one finds the emergence of two power law regimes, with exponents ν_1^C and ν_2^C that have quite distinct values (see Table 1 in the Supplemental Material). At high activity, the tangential forces induce compaction: so, confinement becomes less severe, for the same degree of polymerisation N. In other words, the same channel is effectively larger for polymers at higher activity. Surprisingly, we find that the first exponent ν_1^C is smaller than the bulk exponent $\nu^B(\text{Pe}= 10) \simeq 0.51$. Confinement thus seems to enhance compaction for short, highly active polymers. We may speculate that, under tight confinement conditions, short active chains fold and collapse even more than in bulk due to the presence of hard walls with a rather pronounced curvature. On the other hand, the exponent ν_2^C is found to be compatible with ν^B.

Upon increasing the value of the channel radius R (Fig. 2b), we look again first at the low activity case. We observe that, for Pe= 0.03, the numerical data follow again the passive curve. Notice that, in this case, R_e^C deviates from its passive counterpart a bit earlier (i.e. around $N \approx 100 - 150$) with respect to the onset of the strong confinement regime ($N \approx 300$). The polymer conformation, for such large values of N at Pe= 0.03, is already affected by the activity. At high enough values of N, the two curves display different trends: for passive chains we observe again the onset of the strong confinement $R_e^{C,p} \propto N$ while confined active chains display a power law with a exponent ν_2^C, whose value is, as in the $R = 6\sigma$ case, close to the one measured for ν_1^C. We recover $\nu_1^C = \nu^B(Pe)$ at large values of Pe. Interestingly, the measured value of ν_2^C is consistently smaller than $\nu^B(\text{Pe})$ (see Supplemental Material Table 1), that suggests again that the confinement induces even further compaction. So, in all cases,
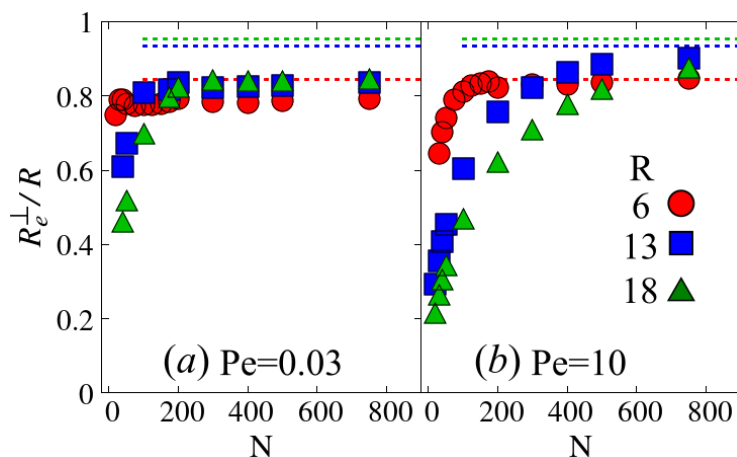
Figure 3: $R_e^\perp/R$ as a function of N for active polymer chains for $R = 6\sigma$ (red circles), 13σ (blue squares) and 18σ (green triangles), and (a) Pe$= 0.03$, (b) Pe$= 10$. Discontinuous lines represents the maximum value for $R_e^\perp$ given by $R - \sigma$.

we can ascribe the behaviour reported to the interplay between activity and confinement: the effects of confinement become dominant over the effects of activity for Pe$\ll 1$, vice-versa for Pe$\gg 1$, at least within a non-negligible window of polymer sizes. Notably, for Pe$\gg 1$, confinement seems to enhance the globule-like character of the tangential propulsion. We get more insight by studying $R_e^\perp$, i.e. the component of R_e^C perpendicular to the channel axis, reported in Fig. 3 as a function of N for various values of R. We observe that, at low activity, $R_e^\perp$ reaches a saturation value at different values of N; for example, under very strong confinement where $R_e^\perp$ is practically constant for all values of N considered. Instead, for $R = 18\sigma$, saturation is reached around $\tilde{N} \approx 200$. Further, at fixed R and high activity, said value is generally reached at larger values of N: for example, for $R = 6\sigma$, we observe a saturation at $\tilde{N} \approx 200$, curiously the same value found before. Instead we do not yet observe a plateau for $R = 18\sigma$. We can thus bring forward an alternative interpretation of the transitions to different regimes in Fig. 2: as the transversal size of the polymers becomes comparable with the channel radius, the active chains can only increase in size in the direction parallel to the channel axis. In practice, if the transverse size is, within the range of values of N considered, always at saturation, than only one regime will be observed. Extending the correspondence to Pe$\gg 1$ and large values of R, the fact that $R_e^\perp$ is not reaching saturation suggests that we are observing a transient regime, enhanced by the presence of the activity. The true strong confinement regime will occur at even higher values of N than the ones considered in this work.

It is also interesting to recast the same data in a different fashion. Indeed, passive flexible polymers display a universal scaling of $R_e^{C,p}$ under confinement [66, 72]: in particular, the ratio of the magnitude of the end-to-end vector under confinement over its bulk counterpart $R_e^{C,p}/R_e^{B,p}$ is a universal function of $R/R_e^{B,p}$. It is thus compelling to assess if such scaling holds for active polymers, where $R_e^B = R_e^B(N, \text{Pe})$ is given again by Eq. (17). We report the result in Fig. 4, where we plot R_e^C/R_e^B as a function of R/R_e^B for Pe$= 0.03, 10$ and different values of R. We observe that, in some regimes of confinement and activity, sufficiently small active polymers behave as their passive counterpart (black line). In contrast, at low confinement or at very high activity, the rescaled data do not follow the passive master curve. Further, long enough polymers deviate from the scaling for any value of Pe or R. More importantly, given this rescaling, the reported data do not collapse on a single universal curve.
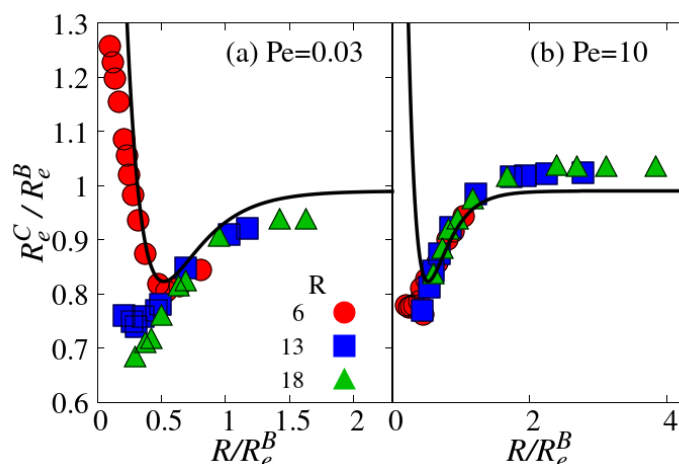
Figure 4: End-to-end distance R_e^C of tangentially active polymers under confinement, scaled over the bulk value R_e^B at the same Pe as a function of R/R_e^B at fixed values of Pe $=0.03$ (panel a) and Pe $=10$ (panel b), for different confinement conditions, $R=6$ (red circles), 13 (blue squares) and 18 (green triangles). The black line refers to the master curve, valid for passive polymers (see SI of Ref. [68] for its functional form).

The universal behaviour of passive flexible polymers under confinement follows the de Gennes blob picture. The characteristic length scale of the blob is either the thermal one or it is set by the confinement; the interplay between the two determines the master curve [65,66,72]. As reported for another active polymer model under confinement [60], a straightforward conclusion is the failure of a blob description, i.e. it is not possible to uniquely define a correlation blob, as other relevant length scales arise. This further hints at the fact that the polymer self-similarity is broken at some non-trivial scale; while the model is different, the effect reported here is similar to what was observed for Active Brownian Polymers [60].

3.2 Radial and angular distributions

We further characterize the polymer conformations by looking at the position and orientations of the chains inside the channel. Specifically, we look at the distribution of the centre of mass within the channel and at the distribution of the angle between the end-to-end vector and the channel axis (see Sec. 2.2).

Concerning the former observable, we focus on four specific cases. In Fig. 5 we report the distribution of the centre of mass positions as a function of the distance from the channel axis, measured in steady state, upon varying N, Pe, and R. In all plots, the channel walls are at $r = R$. We observe that, under strong confinement conditions and weak activity (panel a), the centre of mass of the polymers does not accumulate at the boundary. Large polymers occupy the whole channel, as already pointed out, and the centre of mass is located near the centre of the channel. However, no excess probability at the boundary is found for small polymers.

Looking at the probability distribution of the individual monomers, that we report in the Supplemental Material, one still does not find strong evidence for wall accumulation. Upon increasing R or Pe (panels b-d) the wall accumulation partially reappears. In general, the fact that, upon increasing N, polymers grow in the transverse direction (see Fig. 3), until their transversal size reaches the channel width, forces the centre of mass to be located in the middle of the channel even for Pe$\gg 1$ and in mild confinement. This effect makes flexible active filaments stand out in comparison with active colloids.
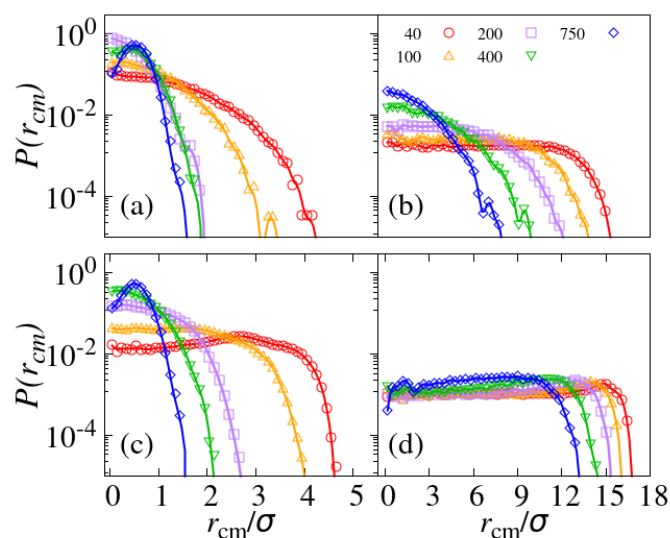
Figure 5: Distribution of the position of the centre of mass of the polymers as a function of the radial distance from the channel centre for different values of N and (a): $R = 6\sigma$, Pe=0.03 (b): $R = 18\sigma$, Pe= 0.03 (c): $R = 6\sigma$, Pe= 10 and (d): $R = 18\sigma$, Pe= 10.

Indeed, active polymers do not accumulate at the channel boundary as long as the size of the channel R is not much larger than the polymer size, in which case the filament can be reasonably approximated by an effective soft colloid.

Further, as anticipated in Sec. 2.3, in order to rationalise the transport properties of tangentially propelled polymers under confinement, we will approximate the polymer as a rigid rod and assume that its orientations is limited. We double check that such approximation is meaningful, assessing how the polymers are oriented with respect to the channel axis (see Sec. 2.2). In Fig. 6, we report the distribution of the angles between the end-to-end vector and the axis of the channel, measured in steady state; the panels (a)-(d) refer to the same cases discussed above. Since the distributions are symmetrics, we report them only between $\theta = 0$ and $\theta = \pi/2$. We remark that, if $\theta = 0$, the end-to-end vector lies parallel to the channel axis; conversely, if $\theta = \pi/2$, the end-to-end vector is perpendicular to it. We observe that, in all four cases, if the polymer size is small with respect to R, the distribution is rather flat; this is expected, as the polymer is not constrained, in this instance, to assume any particular orientation by the confinement. On the contrary, large polymers do preferentially align with the channel axis ($\theta = 0$); the effect is relevant under strong confinement or weak activity conditions. We can thus conclude that the orientations of the polymer are limited only for large values of N and strong confinement conditions, i.e when $R_e^B(N) \simeq R$. The condition is indeed captured by the definition of θ_{max} given in Sec. 2.3.

3.3 Scaling of the correlation time

We further report the correlation time of the chains; this is, as in Refs. [39, 42, 44], the characteristic time of the self-propulsion force and the characteristic time of the active contribution to the diffusion coefficient (see Sec. 2.3).

Interestingly, Fig. 7 shows that the adimensional correlation time $\tau_e^C D_0/\sigma^2$ can be collapsed onto a master curve when plotted as a function of N/Pe. However, with respect to the bulk scaling (dashed line), data under confinement have the same scaling but a different
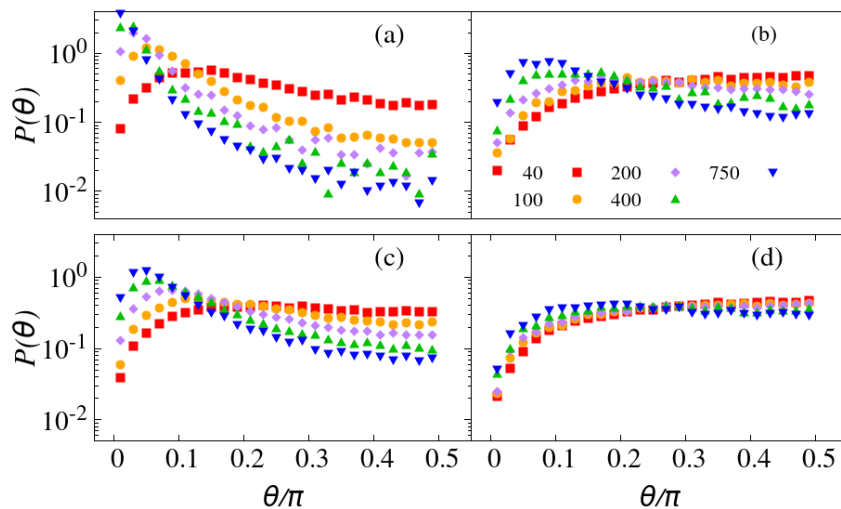
Figure 6: Distribution of the angles between the instantaneous end-to-end vector and the channel axis for different values of N and (a): $R = 6\sigma$, Pe= 0.03 (b): $R = 6\sigma$, Pe= 10 (c): $R = 18\sigma$, Pe= 0.03 (d) $R = 18\sigma$, Pe= 10.
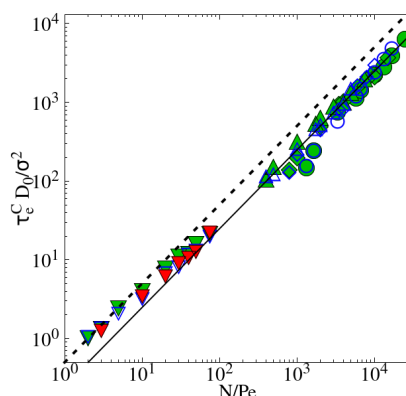

Figure 7: End-to-end vector correlation time under confinement $\tau_e^C D_0/\sigma^2$ as a function of N/Pe for different values of Pe $= 0.03$ (circle), 0.05 (diamond), 0.1 (triangle), 10 (inverted triangle) and confinement R= 6σ (red), 13σ (blue), 18σ (green). Dashed line represents the Bulk ($\tau_0^B = 0.5$) and the continuous line represents the linear fit to data at high values of N/Pe ($\tau_0^C = 0.25$).

prefactor. Indeed, given

$$\tau_e^C D_0/\sigma^2 = \tau_0 \frac{N}{\text{Pe}}, \tag{21}$$

we obtain $\tau_0^C \simeq 0.25$ under confinement, smaller than the bulk value $\tau_0^B \simeq 0.5$. We can recast Eq. (21) in terms of the self-propulsion velocity of the polymer, $v_a = F_a/\gamma$ and of the contour length $L = N\sigma$, as

$$\tau_e = \tau_0 \frac{L}{v_a}. \tag{22}$$

This relation shows that, even under confinement, the polymer is still driven by a "railway motion", as named in the literature [38,44]. The influence of the confinement on the correlation time amounts, thus, to a decrease of the decorrelation time.
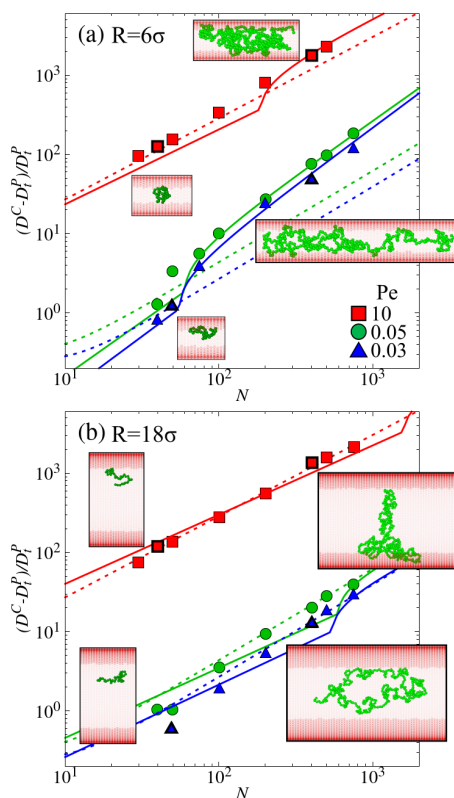
Figure 8: Long time diffusion coefficient as a function of N for different values of Pe$= 0.03$ (blue triangles), 0.05 (green circles), 10 (red squares) and (a) $R = 6\sigma$ (b) $R = 18\sigma$. The symbols refer to simulation data, lines are the theoretical predictions, dashed lines referring to Eq. (19), full lines to Eq. (20).

3.4 Diffusion coefficient predictions via the ABP mapping

In this section, we present results on the transport properties, namely the diffusion coefficient along the channel axis, of active polymers under cylindrical confinement. We will compare the results of the numerical simulations with the predictions of the two models proposed in Sec. 2.3 Eq. (19) and Eq. (20).

We report the comparison in Fig. 8. Again, we focus on two extreme cases of strong confinement $R = 6\sigma$ (panel a) and weak confinement (panel b). The comparison with the theoretical approximations Eq. (19) shows that, under strong confinement, the diffusion coefficient can be enhanced by roughly a factor of 10. We can start rationalizing the result by putting together what we discovered so far. Under confinement, the polymer may experience an elongation with respect to the bulk active case (see Sec. 3.1): in those cases, we should expect an increase of the diffusion coefficient, given by an increase of the force on the centre of mass (see Eq. (12)). Further, for sufficiently large values of N, the polymer also preferentially align with the channel axis, as shown in Fig. 6 and the most notable discrepancies with respect to the bulk data appear when the distribution of the angle θ is not uniform. The geometrical correction, introduced in Sec. 2.3, recapitulates this feature; using it, the predicted diffusion coefficient Eq. (20) nicely agrees with the simulation data. On the other hand, when the confinement is weak, the bulk prediction remains in good agreement with the numerical data at least within the values of N considered, see Fig. 8b. Notice that, for small values of N and Pe$\ll 1$, there is a discrepancy between the simulation data and the bulk prediction. This happens because, in these conditions, R_e^C becomes smaller than R_e^B. This happens also in passive polymers and the discrepancy can be appreciated in Fig. 4. Since for small chains there is no alignment

effect and no difference in the correlation time with respect to the bulk, the difference stems precisely from this discrepancy. Notice also that the discrepancy with the bulk prediction also hints at the fact that the diffusion now increases as a function of N. Further, we may also observe that some of the characteristic features of these active polymers are maintained in confinement as well. Indeed, we report the data in the same fashion as in Ref. [39] in the Supplemental Material. One can appreciate that D_a^C/D_0 (D_0 being the diffusion coefficient of a single monomer) increases upon increasing Pe and, for large values of Pe and weak confinement conditions, the diffusion coefficient is roughly independent on N. However, as already mentioned, the diffusion coefficient increases with N under strong confinement.

4   Conclusions

We report on the conformation and dynamics of tangentially active polymers under cylindrical confinement. Concerning the former, the data highlight the interplay between confinement and self-propulsion: the first induces elongated conformations, the second tends to drive the polymer collapse, as observed in bulk. It is important to stress that the same channel can stand as a mild or strong confinement, depending on the polymer's degree of polymerisation or, in general, on its size. The complex interplay makes non trivial power law regimes emerge at different values of the activity and at different confinement conditions. Further, we show that the universal rescaling, valid for passive polymers under cylindrical confinement, breaks for the active polymers considered here. Following the same argument brought forward by recent literature on active polymers [60], we conclude that the blob picture is broken also for tangentially active polymers: the channel radius cannot be taken as the fundamental length scale of the system.

    We further show that the tendency of active polymers to accumulate at the boundary of the channel is qualitatively different from the colloidal case. In part, if sufficiently long, the polymers tend to expand in the transverse direction and "fill up" the channel (see Fig. 3); however, notably, even for short polymers at high Pe the probability to find the centre of mass at the boundary is only slightly larger than in the bulk of the channel. This may be a feature that makes soft, deformable active filaments stand apart from active colloids. It is intriguing to notice that the accumulation has been observed for many elongated swimmers, such as sperms. As such it would be interesting, from a biophysical perspective, to assess more in detail what are the minimal requirements for wall aggregation, in terms of aspect ratio and filament flexibility, having focused here to relatively large aspect ratios ($N > 40$). Wall aggregation is indeed argued to be important for early stage biofilm formation [73].

    Finally, from the perspective of the dynamics, we show that there is a significant deviation from the bulk, for what concerns the correlation times and the diffusion coefficient, at large values of Pe and strong confinement conditions. For the latter, we propose a correction, based on a geometrical argument. The correction is, in principle, valid for rigid rods, which is not the case for the polymers under investigation. However, as the total active force is almost parallel to R_e, approximating the polymer as its end-to-end vector captures the physics of the system well. Indeed, such a correction yields a good comparison against the simulation results, without any fitting parameter.

    The study of active polymers under confinement may be relevant to better understand and, eventually, mimic, the behaviour of filamentous living organisms. Indeed, many of them live under strong confinement conditions; understanding how they behave may be important to create bio-mimetic soft robots able to burrow and perform tasks, as worms do [74].

Acknowledgments

References

[1] S. Ramaswamy, *Active matter*, J. Stat. Mech.: Theory Exp., 054002 (2017), doi:10.1088/1742-5468/aa6bc5.

[2] M. C. Marchetti, J.-F. Joanny, S. Ramaswamy, T. B. Liverpool, J. Prost, M. Rao and R. A. Simha, *Hydrodynamics of soft active matter*, Rev. Mod. Phys. **85**, 1143 (2013), doi:10.1103/RevModPhys.85.1143.

[3] C. Bechinger, R. Di Leonardo, H. Löwen, C. Reichhardt, G. Volpe and G. Volpe, *Active particles in complex and crowded environments*, Rev. Mod. Phys. **88**, 045006 (2016), doi:10.1103/RevModPhys.88.045006.

[4] L. Rotschild, *Non-random distribution of bull spermatozoa in a drop of sperm suspension*, Nature **198**, 1221 (1963), doi:10.1038/1981221a0.

[5] A. P. Berke, L. Turner, H. C. Berg and E. Lauga, *Hydrodynamic attraction of swimming microorganisms by surfaces*, Phys. Rev. Lett. **101**, 038102 (2008), doi:10.1103/PhysRevLett.101.038102.

[6] P. Sartori, E. Chiarello, G. Jayaswal, M. Pierno, G. Mistura, P. Brun, A. Tiribocchi and E. Orlandini, *Wall accumulation of bacteria with different motility patterns*, Phys. Rev. E **97**, 022610 (2018), doi:10.1103/PhysRevE.97.022610.

[7] V. Kantsler, J. Dunkel, M. Polin and R. E. Goldstein, *Ciliary contact interactions dominate surface scattering of swimming eukaryotes*, Proc. Natl. Acad. Sci. **110**, 1187 (2013), doi:10.1073/pnas.1210548110.

[8] J. Elgeti and G. Gompper, *Wall accumulation of self-propelled spheres*, Europhys. Lett. **101**, 48003 (2013), doi:10.1209/0295-5075/101/48003.

[9] P. Malgaretti and H. Stark, *Model microswimmers in channels with varying cross section*, J. Chem. Phys. **146**, 174901 (2017), doi:10.1063/1.4981886.

[10] M. N. Popescu, W. E. Uspal, A. Domínguez and S. Dietrich, *Effective interactions between chemically active colloids and interfaces*, Acc. Chem. Res. **51**, 2991 (2018), doi:10.1021/acs.accounts.8b00237.

[11] R. G. Winkler and G. Gompper, *The physics of active polymers and filaments*, J. Chem. Phys. **153**, 040901 (2020), doi:10.1063/5.0011466.

[12] D. A. Fletcher and R. D. Mullins, *Cell mechanics and the cytoskeleton*, Nature **463**, 485 (2010), doi:10.1038/nature08908.

[13] D. Saintillan, M. J. Shelley and A. Zidovska, *Extensile motor activity drives coherent motions in a model of interphase chromatin*, Proc. Natl. Acad. Sci. **115**, 11442 (2018), doi:10.1073/pnas.1807073115.

[14] G. H. Koenderink, Z. Dogic, F. Nakamura, P. M. Bendix, F. C. MacKintosh, J. H. Hartwig, T. P. Stossel and D. A. Weitz, *An active biopolymer network controlled by molecular motors*, Proc. Natl. Acad. Sci. **106**, 15192 (2009), doi:10.1073/pnas.0903974106.

[15] A. Sciortino, L. J. Neumann, T. Krüger, I. Maryshev, T. F. Teshima, B. Wolfrum, E. Frey and A. R. Bausch, *Polarity and chirality control of an active fluid by passive nematic defects*, Nat. Mater. **22**, 260 (2023), doi:10.1038/s41563-022-01432-w.

[16] R. Balagam and O. A. Igoshin, *Mechanism for collective cell alignment in myxococcus xanthus bacteria*, PLoS Comput. Biol. **11**, e1004474 (2015), doi:10.1371/journal.pcbi.1004474.

[17] M. K. Faluweki and L. Goehring, *Structural mechanics of filamentous cyanobacteria*, J. R. Soc. Interface **19**, 20220268 (2022), doi:10.1098/rsif.2022.0268.

[18] P. Patra, K. Beyer, A. Jaiswal, A. Battista, K. Rohr, F. Frischknecht and U. S. Schwarz, *Collective migration reveals mechanical flexibility of malaria parasites*, Nat. Phys. **18**, 586 (2022), doi:10.1038/s41567-022-01583-2.

[19] J. Rosko et al., *Cellular coordination underpins rapid reversals in gliding filamentous cyanobacteria and its loss results in plectonemes*, eLife (2024), doi:10.7554/eLife.100768.1.

[20] T. Sugi, H. Ito, M. Nishimura and K. H. Nagai, *C. elegans collectively forms dynamical networks*, Nat. commun. **10**, 683 (2019), doi:10.1038/s41467-019-08537-y.

[21] A. Deblais, S. Woutersen and D. Bonn, *Rheology of entangled active polymer-like T. tubifex worms*, Phys. Rev. Lett. **124**, 188002 (2020), doi:10.1103/PhysRevLett.124.188002.

[22] A. Deblais, A. Maggs, D. Bonn and S. Woutersen, *Phase separation by entanglement of active polymerlike worms*, Phys. Rev. Lett. **124**, 208006 (2020), doi:10.1103/PhysRevLett.124.208006.

[23] C. Nguyen, Y. Ozkan-Aydin, H. Tuazon, D. I. Goldman, M. S. Bhamla and O. Peleg, *Emergent collective locomotion in an active polymer model of entangled worm blobs*, Front. Phys. **9**, 734499 (2021), doi:10.3389/fphy.2021.734499.

[24] T. Heeremans, A. Deblais, D. Bonn and S. Woutersen, *Chromatographic separation of active polymer-like worm mixtures by contour length and activity*, Sci. Adv. **8**, eabj7918 (2022), doi:10.1126/sciadv.abj7918.

[25] V. P. Patil, H. Tuazon, E. Kaufman, T. Chakrabortty, D. Qin, J. Dunkel and M. S. Bhamla, *Ultrafast reversible self-assembly of living tangled matter*, Science **380**, 392 (2023), doi:10.1126/science.ade7759.

[26] R. Dreyfus, J. Baudry, M. L. Roper, M. Fermigier, H. A. Stone and J. Bibette, *Microscopic artificial swimmers*, Nature **437**, 862 (2005), doi:10.1038/nature04090.

[27] L. J. Hill et al., *Colloidal polymers from dipolar assembly of cobalt-tipped CdSe@CdS nanorods*, ACS Nano **8**, 3272 (2014), doi:10.1021/nn406104d.

[28] B. Biswas, R. K. Manna, A. Laskar, P. B. Sunil Kumar, R. Adhikari and G. Kumaraswamy, *Linking catalyst-coated isotropic colloids into "active" flexible chains rnhances their diffusivity*, ACS Nano **11**, 10025 (2017), doi:10.1021/acsnano.7b04265.

[29] D. Nishiguchi, J. Iwasawa, H.-R. Jiang and M. Sano, *Flagellar dynamics of chains of active Janus particles fueled by an AC electric field*, New J. Phys. **20**, 015002 (2018), doi:10.1088/1367-2630/aa9b48.

[30] Y. Ozkan-Aydin, D. I. Goldman and M. S. Bhamla, *Collective dynamics in entangled worm and robot blobs*, Proc. Natl. Acad. Sci. **118**, e2010542118 (2021), doi:10.1073/pnas.2010542118.

[31] E. Zheng, M. Brandenbourger, L. Robinet, P. Schall, E. Lerner and C. Coulais, *Self-oscillation and synchronization transitions in elastoactive structures*, Phys. Rev. Lett. **130**, 178202 (2023), doi:10.1103/PhysRevLett.130.178202.

[32] K. Becker, C. Teeple, N. Charles, Y. Jung, D. Baum, J. C. Weaver, L. Mahadevan and R. Wood, *Active entanglement enables stochastic, topological grasping*, Proc. Natl. Acad. Sci. **119**, e2209819119 (2022), doi:10.1073/pnas.2209819119.

[33] A. Deblais, K. Prathyusha, R. Sinaasappel, H. Tuazon, I. Tiwari, V. P. Patil and M. S. Bhamla, *Worm blobs as entangled living polymers: From topological active matter to flexible soft robot collectives*, Soft Matter **19**, 7057 (2023), doi:10.1039/D3SM00542A.

[34] N. Ganai, S. Sengupta and G. I. Menon, *Chromosome positioning from activity-based segregation*, Nucleic Acids Res. **42**, 4145 (2014), doi:10.1093/nar/gkt1417.

[35] J. Smrek and K. Kremer, *Small activity differences drive phase separation in active-passive polymer mixtures*, Phys. Rev. Lett. **118**, 098002 (2017), doi:10.1103/PhysRevLett.118.098002.

[36] J. Smrek, I. Chubak, C. N. Likos and K. Kremer, *Active topological glass*, Nat. Commun. **11**, 26 (2020), doi:10.1038/s41467-019-13696-z.

[37] A. Kaiser and H. Löwen, *Unusual swelling of a polymer in a bacterial bath*, J. Chem. Phys. **141**, 044903 (2014), doi:10.1063/1.4891095.

[38] R. E. Isele-Holder, J. Elgeti and G. Gompper, *Self-propelled worm-like filaments: Spontaneous spiral formation, structure, and dynamics*, Soft Matter **11**, 7181 (2015), doi:10.1039/C5SM01683E.

[39] V. Bianco, E. Locatelli and P. Malgaretti, *Globulelike conformation and enhanced diffusion of active polymers*, Phys. Rev. Lett. **121**, 217802 (2018), doi:10.1103/PhysRevLett.121.217802.

[40] S. K. Anand and S. P. Singh, *Structure and dynamics of a self-propelled semiflexible filament*, Phys. Rev. E **98**, 042501 (2018), doi:10.1103/PhysRevE.98.042501.

[41] M. Foglino, E. Locatelli, C. Brackley, D. Michieletto, C. Likos and D. Marenduzzo, *Non-equilibrium effects of molecular motors on polymers*, Soft matter **15**, 5995 (2019), doi:10.1039/C9SM00273A.

[42] M. Fazelzadeh, E. Irani, Z. Mokhtari and S. Jabbari-Farouji, *Effects of inertia on conformation and dynamics of tangentially driven active filaments*, Phys. Rev. E **108**, 024606 (2023), doi:10.1103/PhysRevE.108.024606.

[43] C. A. Philipps, G. Gompper and R. G. Winkler, *Tangentially driven active polar linear polymers – An analytical study*, J. Chem. Phys. **157**, 194904 (2022), doi:10.1063/5.0120493.

[44] J.-X. Li, S. Wu, L.-L. Hao, Q.-L. Lei and Y.-Q. Ma, *Nonequilibrium structural and dynamic behaviors of polar active polymer controlled by head activity*, Phys. Rev. Res. **5**, 043064 (2023), doi:10.1103/PhysRevResearch.5.043064.

[45] D. Breoni, C. Kurzthaler, B. Liebchen, H. Löwen and S. Mandal, *Giant activity-induced stress plateau in entangled polymer solutions*, (arXiv preprint) doi:10.48550/arXiv.2310.02929.

[46] P. Malgaretti, E. Locatelli and C. Valeriani, *Coil-to-globule collapse of active polymers: A Rouse perspective*, Mol. Phys. e2384462 (2024), doi:10.1080/00268976.2024.2384462.

[47] M. A. Ubertini, E. Locatelli and A. Rosa, *Universal time and length scales of polar active polymer melts*, ACS Macro Lett. **13**, 1204 (2024), doi:10.1021/acsmacrolett.4c00423.

[48] T. Terakawa, S. Bisht, J. M. Eeftens, C. Dekker, C. H. Haering and E. C. Greene, *The condensin complex is a mechanochemical motor that translocates along DNA*, Science **358**, 672 (2017), doi:10.1126/science.aan6516.

[49] R. K. Manna and P. S. Kumar, *Emergent topological phenomena in active polymeric fluids*, Soft Matter **15**, 477 (2019), doi:10.1039/C8SM01981A.

[50] S. Das and A. Cacciuto, *Dynamics of an active semi-flexible filament in a spherical cavity*, J. Chem. Phys. **151**, 244904 (2019), doi:10.1063/1.5132757.

[51] I. Chubak, S. M. Pachong, K. Kremer, C. N. Likos and J. Smrek, *Active topological glass confined within a spherical cavity*, Macromolecules **55**, 956 (2022), doi:10.1021/acs.macromol.1c02471.

[52] A. Mahajan, W. Yan, A. Zidovska, D. Saintillan and M. J. Shelley, *Euchromatin activity enhances segregation and compaction of heterochromatin in the cell nucleus*, Phys. Rev. X **12**, 041033 (2022), doi:10.1103/PhysRevX.12.041033.

[53] Z. Mokhtari and A. Zippelius, *Dynamics of active filaments in porous media*, Phys. Rev. Lett. **123**, 028001 (2019), doi:10.1103/PhysRevLett.123.028001.

[54] C. Kurzthaler, S. Mandal, T. Bhattacharjee, H. Löwen, S. S. Datta and H. A. Stone, *A geometric criterion for the optimal spreading of active polymers in porous media*, Nat. Commun. **12**, 7088 (2021), doi:10.1038/s41467-021-26942-0.

[55] L. Theeyancheri, S. Chaki, T. Bhattacharjee and R. Chakrabarti, *Migration of active rings in porous media*, Phys. Rev. E **106**, 014504 (2022), doi:10.1103/PhysRevE.106.014504.

[56] Y. Wang et al., *Obstacle-induced giant jammed aggregation of active semiflexible filaments*, Phys. Chem. Chem. Phys. **24**, 23779 (2022), doi:10.1039/D2CP02819K.

[57] M. Fazelzadeh, Q. Di, E. Irani, Z. Mokhtari and S. Jabbari-Farouji, *Active motion of tangentially driven polymers in periodic array of obstacles*, J. Chem. Phys. **159**, 224903 (2023), doi:10.1063/5.0180170.

[58] F. Tan, R. Yan, C. Zhao and N. Zhao, *Translocation dynamics of an active filament through a long-length scale channel*, J. Phys. Chem. B **127**, 8603 (2023), doi:10.1021/acs.jpcb.3c04250.

[59] J. P. Miranda, E. Locatelli and C. Valeriani, *Self-organized states from solutions of active ring polymers in bulk and under confinement*, J. Chem. Theory Comput. **20**, 1636 (2023), doi:10.1021/acs.jctc.3c00818.

[60] S. Das and A. Cacciuto, *Deviations from blob scaling theory for active Brownian filaments confined within cavities*, Phys. Rev. Lett. **123**, 087802 (2019), doi:10.1103/PhysRevLett.123.087802.

[61] C. M. Barriuso Gutiérrez, J. Martín-Roca, V. Bianco, I. Pagonabarraga and C. Valeriani, *Simulating microswimmers under confinement with dissipative particle (hydro) dynamics*, Front. Phys. **10**, 926609 (2022), doi:10.3389/fphy.2022.926609.

[62] C. Li, Q. Chen and M. Ding, *Escape dynamics of active ring polymers in a cylindrical nanochannel*, Soft Matter **20**, 1719 (2024), doi:10.1039/D3SM01524F.

[63] D. Marenduzzo, C. Micheletti and E. Orlandini, *Biopolymer organization upon confinement*, J. Phys.: Condens. Matter **22**, 283102 (2010), doi:10.1088/0953-8984/22/28/283102.

[64] M. Muthukumar, *Polymers under confinement*, Adv. Chem. Phys. **149**, 129 (2012), doi:10.1039/C9SM01141B.

[65] L. Dai, C. B. Renner and P. S. Doyle, *The polymer physics of single DNA confined in nanochannels*, Adv. Colloid Interface Sci. **232**, 80 (2016), doi:10.1016/j.cis.2015.12.002.

[66] G. Morrison and D. Thirumalai, *The shape of a flexible polymer in a cylindrical pore*, J. Chem. Phys. **122**, 194907 (2005), doi:10.1063/1.1903923.

[67] K. Kremer and G. S. Grest, *Dynamics of entangled linear polymer melts: A molecular-dynamics simulation*, J. Chem. Phys. **92**, 5057 (1990), doi:10.1063/1.458541.

[68] E. Locatelli, V. Bianco, C. Valeriani and P. Malgaretti, *Nonmonotonous translocation time of polymers across pores*, Phys. Rev. Lett. **131**, 048101 (2023), doi:10.1103/PhysRevLett.131.048101.

[69] S. Plimpton, *Fast parallel algorithms for short-range molecular dynamics*, J. Comput. Phys. **117**, 1 (1995), doi:10.1006/jcph.1995.1039.

[70] B. ten Hagen, S. van Teeffelen and H. Löwen, *Brownian motion of a self-propelled particle*, J. Phys.: Condens. Matter **23**, 194119 (2011), doi:10.1088/0953-8984/23/19/194119.

[71] P. Malgaretti and J. Harting, *Transport of neutral and charged nanorods across varying-section channels*, Soft Matter **17**, 2062 (2021), doi:10.1039/D0SM02045A.

[72] Y.-L. Chen, M. Graham, J. De Pablo, G. Randall, M. Gupta and P. Doyle, *Conformation and dynamics of single DNA molecules in parallel-plate slit microchannels*, Phys. Rev. E **70**, 060901 (2004), doi:10.1039/D0SM02045A.

[73] J. Jara et al., *Self-adaptation of pseudomonas fluorescens biofilms to hydrodynamic stress*, Front. Microbiol. **11**, 588884 (2021), doi:10.3389/fmicb.2020.588884.

[74] A. Kudrolli and B. Ramirez, *Burrowing dynamics of aquatic worms in soft sediments*, Proc. Natl. Acad. Sci. **116**, 25569 (2019), doi:10.1073/pnas.1911317116.